


Article

On Symmetry Properties of The Corrugated Graphene System

Mihal Pudlak ¹, Jan Smotlacha ² and Rashid Nazmitdinov ^{2,3,*} ¹ Institute of Experimental Physics, Watsonova 47, 04001 Košice, Slovakia² BLTP, Joint Institute for Nuclear Research, 141980 Dubna, Moscow Region, Russia³ BLTP, Dubna University, 141982 Dubna, Moscow Region, Russia

* Correspondence: rashid@theor.jinr.ru

Received: 20 February 2020; Accepted: 24 March 2020; Published: 3 April 2020



Abstract: The properties of the ballistic electron transport through a corrugated graphene system are analysed from the symmetry point of view. The corrugated system is modelled by a curved surface (an arc of a circle) connected from both sides to flat sheets. The spin–orbit couplings, induced by the curvature, give rise to equivalence between the transmission (reflection) probabilities of the transmitted (reflected) electrons with the opposite spin polarisation, incoming from opposite system sides. We find two integrals of motion that explain the chiral electron transport in the considered system.

Keywords: graphene; ripple; transport; symmetry

1. Introduction

It appears that graphene possesses a remarkable stretchability. For example, the DFT and molecular dynamics simulations predict that it can be stretched up to about 20–30%, without being damaged [1]. The experimental measurements demonstrate a good agreement with the theoretical estimations, while the robust engineering results indicate on sample-wide elastic strain $\sim 6\%$ [2]. Evidently, transforming the flat surface to the curved one, one creates the strain that affects the graphene properties. This fact suggests that, by altering the stretchability, one might tune electronic and transport properties of the graphene sheet.

Recent experimental techniques enable demonstrating evidently a spatial variation of graphene and its direct consequences. For example, ripples can be formed by means of the electrostatic manipulation without any change of doping [3]. Periodically rippled graphene can be fabricated by the epitaxial technique (e.g., [4]). In this case, in contrast to free-standing graphene, a strong modification of the electronic structure of graphene is observed, which gives rise to localised phonon [5] and plasmon [6] modes. Periodic nanoripples can be created as well by means of the chemical vapour deposition [7]. It is found that ripples, acting as potential barriers, yield the localisation of charged carriers [8]. The potential surface variations could reach the figure of 20–30 meV. Similar independent prediction has been done in the study of Klein collimation by the rippled graphene superlattice [9]. In this model, the hybridisation between the π - and σ -orbitals creates the potential barrier between the flat and curved graphene pieces. The barrier value could reach $\Delta\varepsilon \approx 24$ meV at the ripple radius $R = 12\text{Å}$. This fact provides the confidence in the vitality and the validity of our model (outlined in Section 2) and following analyses its symmetry properties, presented in our paper.

Indeed, the lattice deformation changes the distance between ions, p_z orbital orientation, and is leading to shift of the on-site energies of p_z orbitals. This affects the effective Dirac equation that could simulate the low energy electron states as a result of a deformation-induced gauge field [10]. The surface curvature modulates also the hopping parameter in the tight-binding approach [10,11].

Moreover, it enhances as well the effect of the spin–orbit coupling [12], usually neglected in flat carbon-based systems.

Recently, it is predicted that rippled graphene could lead to the spin selectivity effect for the ballistic electrons [13,14] in virtue of the curvature-induced spin–orbit couplings (see details in [12,13,15–17]). As a result, it is shown that at the particular energy values the ballistic electrons with the one spin polarisation can travel through periodically repeated ripples without any reflection. At the same time, electrons with the opposite spin polarisation are fully reflected. Once we change the flow direction through the considered system, the situation becomes inverse. It is noteworthy that different experiments of a spin selective electron transmission through biomolecules has been discussed recently in Ref. [18]. In this review, the authors claimed that this phenomenon implies that chirality and spin may play an important role in biology.

In mesoscopic systems, symmetries are key points that allow to illuminate essential features of finite quantum systems (e.g., [19,20]). The basic goal of this paper is to elucidate the above discussed phenomenon from point of view of the symmetry properties of the considered system.

2. Basic Physics of The Corrugated Graphene

In our consideration, the corrugated graphene structure consists of a rippled graphene connected to two flat graphene sheets (see Figure 1).

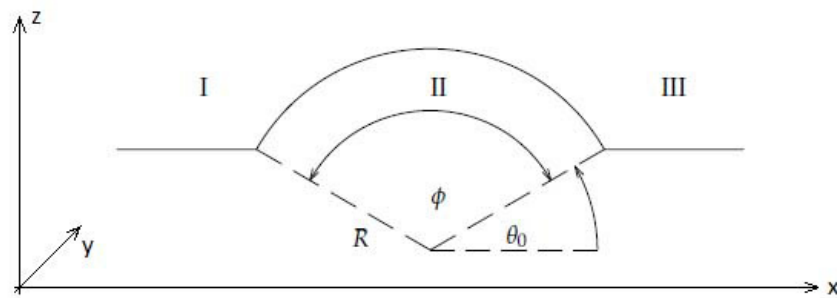


Figure 1. The corrugated graphene system. There are two flat surfaces: Region I, defined in the intervals $-\infty < x < -R \cos \theta_0$; and Region III, defined in the intervals $R \cos \theta_0 < x < \infty$. A ripple is modelled by an arc of a circle (Region II) of radius R , defined as $-R \cos \theta_0 < x < R \cos \theta_0$. At $\theta_0 = 0$, the ripple is a half of the nanotube, while at $\theta_0 = \pi/2$ the ripple does not exist. The angle $\phi = \pi - 2\theta_0$. Here, we have $-\infty < y < \infty$. We keep the translational invariance along the y -axis, which is chosen as the symmetry and the quantisation axis.

For analysis of the curved graphene surface, we recapitulate the major results [17] obtained for armchair CNTs. In this case, only the interaction between nearest neighbour atoms is considered. The analysis is done in an effective mass approximation for the point K, in the vicinity of the Fermi level $E = 0$. A similar approach can be applied for K' point.

The Hamiltonian of the nanotube has the following form in the effective mass approximation [12]

$$H_r = \gamma(\tau_x \hat{\pi}_x + \tau_y \hat{\pi}_y) \otimes I - \lambda_y \tau_y \otimes \sigma_x(\vec{r}) - \xi_x \tau_x \otimes \sigma_y. \quad (1)$$

Here, the operators $\hat{\pi}_x = -i \frac{\partial}{R \partial \theta}$, $\hat{\pi}_y = -i \frac{\partial}{\partial y}$, $\sigma_x(\vec{r}) = \sigma_x \cos \theta - \sigma_z \sin \theta$, and $\xi_x = 2\delta\gamma p/R$, $\lambda_y = \delta\gamma'/4R$. The Pauli matrices $\sigma_{x,y}$ act in the spin space. The matrices $\tau_{x,y}$ act on the sublattice degree of freedom. The Pauli matrix τ_i is called the "pseudospin", to distinguish it from the real electron spin.

The following notations are used: $\gamma = -\sqrt{3}V_{pp}^\pi a/2 = \sqrt{3}\gamma_0 a/2$, $\gamma' = \sqrt{3}(V_{pp}^\sigma - V_{pp}^\pi)a/2 = \gamma_1 a$, $p = 1 - 3\gamma'/8\gamma$; where V_{pp}^σ and V_{pp}^π are the transfer integrals for σ - and π -orbitals, respectively, in a flat graphene. The distance d between atoms in the unit cell determines the length of the primitive translation vector $a = \sqrt{3}d \simeq 2.46 \text{ \AA}$. For numerical illustration, we assume that $\gamma_0 = -V_{pp}^\pi \approx 3 \text{ eV}$

and $\gamma_1 \approx 8$ eV (see, e.g., [12]). The intrinsic source of the spin-orbit coupling $\delta = \Delta/3\epsilon_{\pi\sigma}$ is defined by means of the quantity

$$\Delta = i\frac{3\hbar}{4m^2c^2} \left\langle x \left| \frac{\partial V}{\partial x} p_y - \frac{\partial V}{\partial y} p_x \right| y \right\rangle, \quad (2)$$

where V is the atomic potential and $\epsilon_{\pi\sigma} = \epsilon_{2p}^\pi - \epsilon_{2p}^\sigma$. Here, the energies ϵ_{2p}^π and ϵ_{2p}^σ denote the energies of π - and σ -orbitals, respectively. We recall that σ -orbitals are localised between carbon atoms, while π -orbitals are directed perpendicular to the nanotube surface.

With the aid of the method discussed in [13,17], one obtains the eigenvalues of the Hamiltonian in Equation (1)

$$E = \kappa E_\pm, \quad \kappa = \pm 1, \quad (3)$$

where $\kappa = +1(-1)$ is associated with the conductance (valence) band, and the energies E_\pm are defined as

$$E_\pm = \sqrt{t_m^2 + t_y^2 + \lambda_y^2 + \lambda_x^2 \pm 2\sqrt{\lambda_x^2(t_m^2 + \lambda_y^2) + t_y^2\lambda_y^2}}. \quad (4)$$

Here, $t_m = m\gamma/R$, $t_y = \gamma k_y$, $\lambda_x = \gamma(1/2 + 2\delta p)/R$, and m is a magnetic quantum number (see details in [13,17]). Due to the curvature-induced spin-orbit coupling spin is no anymore a good quantum number. The eigenstates of Equation (1) are characterised by a quantum number $s = \pm 1$, and have the following form

$$\Phi_{m,k_y}^{s=\pm 1}(\theta, y) = e^{im\theta} e^{ik_y y} N_\pm \begin{bmatrix} \kappa(\cos\theta/2 A_\pm - \sin\theta/2 B_\pm) \\ \kappa(\sin\theta/2 A_\pm + \cos\theta/2 B_\pm) \\ \cos\theta/2 C_\pm - \sin\theta/2 D_\pm \\ \sin\theta/2 C_\pm + \cos\theta/2 D_\pm \end{bmatrix}, \quad (5)$$

where

$$D_\pm = \frac{\lambda_y \lambda_x \pm \sqrt{\lambda_x^2(t_m^2 + \lambda_y^2) + t_y^2\lambda_y^2}}{it_m \lambda_x - t_y \lambda_y}, \quad (6)$$

$$A_\pm = \frac{1}{E_\pm} (t_m - it_y + i(\lambda_y + \lambda_x) D_\pm), \quad (7)$$

$$B_\pm = \frac{1}{E_\pm} [(t_m - it_y) D_\pm + i(\lambda_y - \lambda_x)], \quad (8)$$

$$C_\pm = 1, \quad (9)$$

and N_\pm is a normalisation constant

$$N_\pm^2 = \frac{t_y^2 \lambda_y^2 + t_m^2 \lambda_x^2}{2 \left[\left(\lambda_y \lambda_x \pm \sqrt{\lambda_x^2(t_m^2 + \lambda_y^2) + t_y^2\lambda_y^2} \right)^2 + t_y^2 \lambda_y^2 + t_m^2 \lambda_x^2 \right]}. \quad (10)$$

Generally, the relations $|A_\pm| = |D_\pm|$ and $|B_\pm| = |C_\pm|$ are fulfilled.

The solution for a flat graphene is well known (e.g., [21,22]). Near the center of each valley (the point K or K') electron dispersion is determined by the Dirac-type Hamiltonian

$$H_f = \gamma(\tau_x \hat{k}_x + \tau_y \hat{k}_y) \otimes I, \quad (11)$$

where again the Pauli matrices $\tau_{x,y}$ act on the sublattice degrees of freedom, I is 2×2 unity matrix acting in the spin space, with $\hat{k} = -i(\partial/\partial x, \partial/\partial y)$. The eigenvalues and eigenstates of the flat graphene Hamiltonian are

$$E = \kappa \gamma \sqrt{k_x^2 + k_y^2}, \quad \kappa = \pm 1, \quad (12)$$

$$\Psi_k^\sigma(x, y) = \frac{1}{2} \begin{pmatrix} \kappa e^{-i\varphi} \\ 1 \end{pmatrix} \otimes \begin{pmatrix} 1 \\ \sigma i \end{pmatrix} e^{ik \cdot r}, \quad \sigma = \pm, \quad (13)$$

where $e^{-i\varphi} = (k_x - ik_y) / \sqrt{k_x^2 + k_y^2}$, $\mathbf{k} = (k_x, k_y)$, $\mathbf{r} = (x, y)$, and $k = \sqrt{k_x^2 + k_y^2}$. The spin degeneracy is taken into account. In our consideration, the states with the spin up and down are the eigenstates of the operator σ_y . The above describe solutions are used to calculate the electron transmission through the corrugated graphene. We recall that, in rippled graphene, the symmetries related to the spin degree of freedom and to the angular momentum are not conserved [13,17].

3. Symmetries

To illuminate specific symmetries of our system, we have to identify the corresponding operators that act within one valley only. Evidently, these operators should act on the A and B sublattices of the honeycomb lattice.

3.1. The Operator $\hat{S}_t = \tau_y \otimes i\sigma_y C$

The spin-orbit coupling implies that one of the symmetries should be related to the time-reverse symmetry operator $\mathcal{T} = i\sigma_y C$ with C the operator of complex conjugation (see, e.g., [23,24]). However, the operator \mathcal{T} does not commute neither with the Hamiltonian of the flat graphene in Equation (11) or with the Hamiltonian of the ripple in Equation (1). Taking into account the “pseudospin” degree of freedom, we observe consequently that the operator $\hat{S}_t = \tau_y \otimes \mathcal{T}$ commutes with the both Hamiltonians

$$[\hat{S}_t, H_f] = 0, \quad [\hat{S}_t, H_r] = 0. \quad (14)$$

Let us investigate the properties of this operator with respect to the eigenfunctions of the Hamiltonian H_f (H_r) described in Section 2. For the sake of convenience, we introduce the following equivalent definitions: $\Psi_k^\sigma(x, y) \equiv \langle \mathbf{r} | \sigma, \mathbf{k} \rangle$, $\sigma = (+/-) \Leftrightarrow \sigma = (\uparrow / \downarrow)$. As a result, for the wave function, associated with the flat graphene sheet, we have

$$\left. \begin{aligned} \hat{S}_t | \uparrow \pm \mathbf{k} \rangle &= \pm e^{i\varphi} | \downarrow \mp \mathbf{k} \rangle \\ \hat{S}_t | \downarrow \pm \mathbf{k} \rangle &= \mp e^{i\varphi} | \uparrow \mp \mathbf{k} \rangle \end{aligned} \right\} \Rightarrow S_t^2 = 1, \quad (15)$$

i.e., the operator \hat{S}_t has two eigenvalues $+1$ and -1 . Since the phase $e^{i\varphi}$ does not affect our results, hereafter, we omit it in our calculations.

Any ket $|\psi\rangle$ can be expressed as

$$|\psi\rangle = \frac{1}{2} [(1 + \hat{S}_t) |\psi\rangle + (1 - \hat{S}_t) |\psi\rangle] = |\psi_+\rangle + |\psi_-\rangle, \quad (16)$$

where

$$|\psi_+\rangle = \frac{1 + \hat{S}_t}{2} |\psi\rangle, \quad |\psi_-\rangle = \frac{1 - \hat{S}_t}{2} |\psi\rangle, \quad (17)$$

with the property $\hat{S}_t |\psi_\pm\rangle = \pm |\psi_\pm\rangle$. In our particular case, we can form four types of the wave functions:

$$|\psi_\pm\rangle = \frac{1 \pm \hat{S}_t}{2} | \uparrow + \mathbf{k} \rangle = \frac{1}{2} (| \uparrow + \mathbf{k} \rangle \pm | \downarrow - \mathbf{k} \rangle), \quad (18)$$

$$|\phi_\pm\rangle = \frac{1 \pm \hat{S}_t}{2} | \downarrow + \mathbf{k} \rangle = \frac{1}{2} (| \downarrow + \mathbf{k} \rangle \mp | \uparrow - \mathbf{k} \rangle). \quad (19)$$

Thus, for the plane graphene sheet the full set of the operator \hat{S}_t consists of the wave functions in Equations (18) and (19). These wave functions contain the equal mixture of the spin up and down states, associated with electrons that move in opposite directions of our structure.

Since for the curved graphene we use the eigenstates of the CNT, a complete set of quantum numbers consists of the magnetic quantum number m and the wave number k_y . In this case, we introduce the equivalent notations $\Phi_{m,k_y}^s(\theta) \equiv \langle \theta | s, m, k_y \rangle$. The action of the operator \hat{S}_t on the wave function in Equation (5), associated with the nanotube, yields

$$\left. \begin{aligned} \hat{S}_t |s = +, \pm m, \pm k_y\rangle &= iB_+^* |s = +, \mp m, \mp k_y\rangle \\ \hat{S}_t |s = -, \pm m, \pm k_y\rangle &= iB_-^* |s = -, \mp m, \mp k_y\rangle \end{aligned} \right\} \Rightarrow S_t^2 = 1, \quad (20)$$

since $|B_{\pm}|^2 = 1$ [see Equation (8)]. Applying the same arguments [see Equations (16) and (17)], we obtain

$$|\chi_{\pm}\rangle = \frac{1 \pm \hat{S}_t}{2} |s = +, m, k_y\rangle = \frac{1}{2} (|s = +, m, k_y\rangle \pm iB_+^* |s = +, -m, -k_y\rangle), \quad (21)$$

$$|\varphi_{\pm}\rangle = \frac{1 \pm \hat{S}_t}{2} |s = -, m, k_y\rangle = \frac{1}{2} (|s = -, m, k_y\rangle \pm iB_-^* |s = -, -m, -k_y\rangle). \quad (22)$$

Having the symmetry properties of the wave functions of the different elements of our structure, we are ready to elucidate the symmetry properties of the transmission and reflection probabilities. Equating the wave functions Ψ , Φ at points $x = -R \cos \theta_0$ (the boundary between Regions I and II), and $x = R \cos \theta_0$ (the boundary between Regions II and III), we define the unknown reflection and transmission amplitudes r_{α}^{β} , t_{α}^{β} ($\alpha, \beta = \uparrow, \downarrow$). In these amplitudes, the upper (bottom) index denotes the spin polarisation of the incoming (outgoing) (reflected and transmitted) electron. For the sake of discussion, in our model, electrons move from the left to the right direction. As a result, at the boundary between Regions I and II for the electron, which moves from the left side with the spin up polarisation, we have:

$$\Psi_{k_x, k_y}^+(x) + r_L(\phi)_{\uparrow}^{\uparrow} \Psi_{-k_x, k_y}^+(x) + r_L(\phi)_{\downarrow}^{\uparrow} \Psi_{-k_x, k_y}^-(x) = \quad (23)$$

$$a_+ \Phi_{m_+, k_y}^+(\theta) + b_+ \Phi_{-m_+, k_y}^+(\theta) + a_- \Phi_{m_-, k_y}^-(\theta) + b_- \Phi_{-m_-, k_y}^-(\theta); \quad x = -R \cos \theta_0, \theta = -\phi/2.$$

The unknown coefficients $a_{(+/-)}$, $b_{(+/-)}$ characterise transport properties of the electron transfer across the rippled region. The wave numbers m_+ and m_- are determined by the equation

$$m_{\pm} = \frac{R}{\gamma} \sqrt{E^2 - t_y^2 - \lambda_y^2 + \lambda_x^2 \mp 2\sqrt{\lambda_x^2(E^2 - t_y^2) + \lambda_y^2 t_y^2}}, \quad (24)$$

where $E = \gamma k$ ($E > 0$) is the electron energy. At the boundary between Regions II and III, we have the following conditions

$$a_+ \Phi_{m_+, k_y}^+(\theta) + b_+ \Phi_{-m_+, k_y}^+(\theta) + a_- \Phi_{m_-, k_y}^-(\theta) + b_- \Phi_{-m_-, k_y}^-(\theta) = \quad (25)$$

$$t_L(\phi)_{\uparrow}^{\uparrow} \Psi_k^+(x) + t_L(\phi)_{\downarrow}^{\uparrow} \Psi_k^-(x); \quad x = R \cos \theta_0, \theta = \phi/2.$$

The system of Equations (23) and (25) determine the coefficients $r_L(\phi)_{\alpha}^{\beta}$ and $t_L(\phi)_{\alpha}^{\beta}$. Acting by the operator \hat{S}_t on these equations, we obtain:

- at the boundary between Region I and II

$$\begin{aligned} &\Psi_{-k_x, -k_y}^-(x) - r_L(\phi)_{\uparrow}^{\uparrow} \Psi_{k_x, -k_y}^-(x) + r_L(\phi)_{\downarrow}^{\uparrow} \Psi_{k_x, -k_y}^+(x) = \\ &ia_+^* B_+^*(m_+, k_y) \Phi_{-m_+, -k_y}^+(\theta) + ib_+^* B_+^*(-m_+, k_y) \Phi_{m_+, -k_y}^+(\theta) + \\ &+ ia_-^* B_-^*(m_-, k_y) \Phi_{-m_-, -k_y}^-(\theta) + ib_-^* B_-^*(-m_-, k_y) \Phi_{m_-, -k_y}^-(\theta); \quad x = R \cos \theta_0, \theta = -\phi/2; \end{aligned} \quad (26)$$

- at the boundary between Region II and III

$$\begin{aligned} & ia_+^* B_+^*(m_+, k_y) \Phi_{-m_+, -k_y}^+(\theta) + ib_+^* B_+^*(-m_+, k_y) \Phi_{m_+, -k_y}^+(\theta) + \\ & + ia_-^* B_-^*(m_-, k_y) \Phi_{-m_-, -k_y}^-(\theta) + ib_-^* B_-^*(-m_-, k_y) \Phi_{m_-, -k_y}^-(\theta) = \\ & t_L(\phi) \uparrow^* \Psi_{-k}^-(x) - t_L(\phi) \downarrow^* \Psi_{-k}^+(x); \quad x = -R \cos \theta_0, \theta = \phi/2. \end{aligned} \quad (27)$$

Next, we consider the equations that determine the coefficients $r_R(\phi)_\alpha^\beta$ and $t_R(\phi)_\alpha^\beta$ for the electron that moves from the right to the left side with the down spin polarisation. Namely, we have:

- at the boundary between Regions II and III

$$\begin{aligned} & \Psi_{-k_x, -k_y}^-(x) + r_R(\phi) \downarrow \Psi_{k_x, -k_y}^-(x) + r_R(\phi) \uparrow \Psi_{k_x, -k_y}^+(x) = \\ & \tilde{a}_+ \Phi_{m_+, -k_y}^+(\theta) + \tilde{b}_+ \Phi_{-m_+, -k_y}^+(\theta) + \tilde{a}_- \Phi_{m_-, -k_y}^-(\theta) + \tilde{b}_- \Phi_{-m_-, -k_y}^-(\theta); \quad x = R \cos \theta_0, \theta = \phi/2; \end{aligned} \quad (28)$$

- at the boundary between Regions I and II

$$\begin{aligned} & \tilde{a}_+ \Phi_{m_+, -k_y}^+(\theta) + \tilde{b}_+ \Phi_{-m_+, -k_y}^+(\theta) + \tilde{a}_- \Phi_{m_-, -k_y}^-(\theta) + \tilde{b}_- \Phi_{-m_-, -k_y}^-(\theta) = \\ & t_R(\phi) \downarrow \Psi_{-k_x, -k_y}^-(x) + t_R(\phi) \uparrow \Psi_{-k_x, -k_y}^+(x); \quad x = -R \cos \theta_0, \theta = -\phi/2. \end{aligned} \quad (29)$$

From the comparison of Equations (26) and (27) with Equations (28) and (29), it follows that the coefficients $r_R(\phi)_\alpha^\beta$ and $t_R(\phi)_\alpha^\beta$ of Equations (28) and (29) can be expressed in the following form

$$r_R(\phi) \downarrow = -r_L(-\phi) \uparrow^*; \quad r_R(\phi) \uparrow = r_L(-\phi) \downarrow^*; \quad (30)$$

and

$$t_R(\phi) \downarrow = -t_L(-\phi) \uparrow^*; \quad t_R(\phi) \uparrow = -t_L(-\phi) \downarrow^*. \quad (31)$$

As a result, we obtain for the reflection probabilities

$$|r_R(\phi) \downarrow|^2 = |r_L(-\phi) \uparrow|^2; \quad |r_R(\phi) \uparrow|^2 = |r_L(-\phi) \downarrow|^2, \quad (32)$$

while for the transmission probabilities we have

$$|t_R(\phi) \downarrow|^2 = |t_L(-\phi) \uparrow|^2; \quad |t_R(\phi) \uparrow|^2 = |t_L(-\phi) \downarrow|^2. \quad (33)$$

We have similar probabilities for the electron motion with the spin up polarisation from the right to the left side

$$|r_R(\phi) \uparrow|^2 = |r_L(-\phi) \downarrow|^2; \quad |r_R(\phi) \downarrow|^2 = |r_L(-\phi) \uparrow|^2, \quad (34)$$

and, consequently, for the transmission probabilities

$$|t_R(\phi) \uparrow|^2 = |t_L(-\phi) \downarrow|^2; \quad |t_R(\phi) \downarrow|^2 = |t_L(-\phi) \uparrow|^2. \quad (35)$$

From these results, it follows that the operator \hat{S}_t does not involve the other valley, i.e., QED. However, it interchanges the sign of the vector \mathbf{k} and the electron spin polarisation in the flat part of the considered graphene structure. In the rippled graphene region, it changes $m_\pm \rightarrow -m_\pm$ and the sign of the k_y component: $k_y \rightarrow -k_y$. We conclude that the operator S_t acts like a time-reversal operator in the single valley.

3.2. The Operator $\hat{S}_{ch} = \tau_x \otimes \sigma_y$

We recall that it was found in Refs. [13,14] that the electron scattering in the superlattice, created by periodically repeated elements, has a curious behaviour. Note that in this way we mimic

periodically rippled graphene as a set curvatures between flat graphene areas (e.g., see Figure 1 and the corresponding discussion in Ref. [14]). One element of the superlattice gives rise to the dominance of the electron transmission with a certain spin polarisation. While this effect is small for a few ripples, it defines the perfect transmission for electrons with the one spin polarisation and the perfect reflection for electrons with the opposite spin polarisation in the case of hundreds of ripples. As a result, we find the optimal angle values for the ripple that ensures the perfect transmission at relatively large number of elements $N \gg 1$ in the superlattice. Note that the transmission depends on the ripple radius and the spin-orbit coupling strengths (see details in [14]). It is noteworthy that transmitted electrons with different spin orientation choose different channels characterised by the quantum number $s = \pm 1$ [13]. This fact implies the existence of the additional symmetry that is fundamental for this feature.

To give an insight into this symmetry, we consider the case $k_y = 0$, when the spectrum in Equation (4) and the eigenspinors are particular simple. In this case, Equations (3) and (4) are reduced to the form

$$E = \pm(\mathcal{D} \pm \lambda_x), \quad (36)$$

where $\mathcal{D} = \sqrt{\lambda_y^2 + t_m^2}$ and $t_m = \frac{\gamma}{R}m$. For the rippled (arc) piece (see Figure 1), there are four eigenenergies

$$E = \begin{cases} \mathcal{E}_1 = \lambda_x + \mathcal{D} \\ \mathcal{E}_2 = \lambda_x - \mathcal{D} \\ \mathcal{E}_3 = -\lambda_x + \mathcal{D} \\ \mathcal{E}_4 = -\lambda_x - \mathcal{D} \end{cases} \quad (37)$$

The connection between the energy and the quantum number m can be formulated in the form

$$m \Rightarrow m_s = \pm \frac{R}{\gamma} \sqrt{(sE - \lambda_x)^2 - \lambda_y^2}, \quad s = \pm 1, \quad (38)$$

that determines four possible values of the quantum number m . Here, we introduce the additional quantum number s that characterises our eigenstates. Note that in Equation (38) the sign of the quantum number s depends on the sign of the energy E . In particular, the following relations take place

$$E > 0 : \Longleftrightarrow \begin{cases} s = +1, & \mathcal{E}_1 > 0 \\ s = +1, & \text{if } \mathcal{E}_2 > 0 \\ s = -1, & \text{if } \mathcal{E}_3 > 0 \end{cases} \quad (39)$$

On the other hand, at $E < 0$, the branches \mathcal{E}_3 and \mathcal{E}_4 have the quantum number $s = +1$, while the branch \mathcal{E}_2 is characterised by the quantum number $s = -1$.

At a fixed electron energy $E (E > 0)$, Equations (37), (38), and (39), establish the connection between the energies $\mathcal{E}_j (j = 1, 2, 3)$ and the magnetic quantum number m with the quantum number s

$$\mathcal{E}_1, \mathcal{E}_2 \rightarrow \pm t_{m_{+1}} \Longleftrightarrow s = +1, \quad (40)$$

$$\mathcal{E}_3 \rightarrow \pm t_{m_{-1}} \Longleftrightarrow s = -1. \quad (41)$$

We recall that the angular momentum is not conserved. As a result, the eigenfunction is the mixture of the eigenfunctions in Equation (5) at a given energy (see Figure 2). The energy branches in Equation (37) with the same quantum number s repel each other, while there is a crossing of the branches with the different s (see Figures 2 and 3). The anticrossings yield the energy gaps $= 2\lambda_y$ indicated by the arrows (see the insets in Figures 2 and 3). As a result, the energy gaps give rise to evanescent modes at energies $\lambda_x - \lambda_y < |E| < \lambda_x + \lambda_y$ in our system.

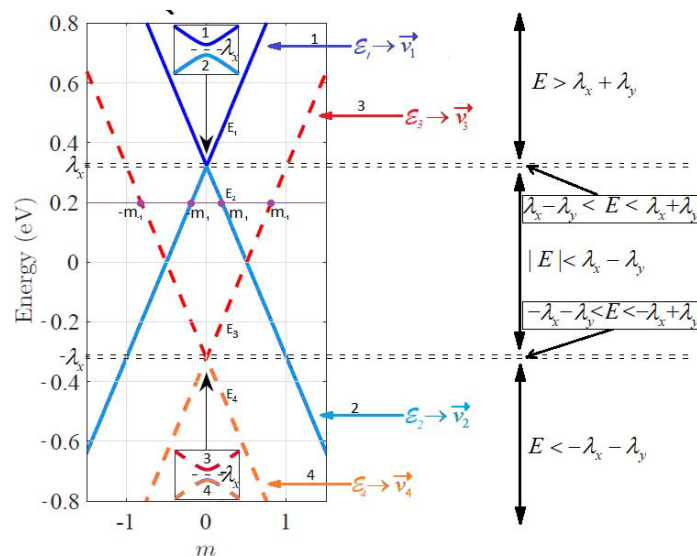


Figure 2. The spectrum in Equation (4) ($k_y = 0$) versus the magnetic quantum number m . The non-quantised values $\pm m_{s=\pm 1}$ at the energy $E = 0.2$ eV (thin horizontal line that mimics the Fermi energy) are indicated at the crossing of the energy branches with different s . Symbols E_1, E_2, E_3, E_4 are used to guide the eyes on the formal solutions (straight lines) defined by Equation (36), irrespective of the sign of the quantum number s . In contrast, there is anticrossing of the energy branches with the same quantum number $s = +1$ for the pair $(\mathcal{E}_1, \mathcal{E}_2)$ at $E > 0$. Similar anticrossing occurs at $E < 0$, when the pair $(\mathcal{E}_3, \mathcal{E}_4)$ has the same quantum number $s = +1$. These anticrossings are caused by the term λ_y in the Hamiltonian in Equation (1), which creates the energy gaps $2\lambda_y$ near the energy $E = \pm \lambda_x$ (see [13,17]). The following parameters are used: $R = 10$ Å, $\delta = 0.01$, $p = 0.1$, $\gamma = (4.5 \cdot 1.42)$ eV · Å, $\gamma' = \frac{8}{3}\gamma$. These parameters define the values of the spin-orbit coupling strengths: $\lambda_y = \delta\gamma'/4R = 0.0043$ eV, $\lambda_x = \gamma(1/2 + 2\delta p)/R = 0.32$ eV (see Section 2).

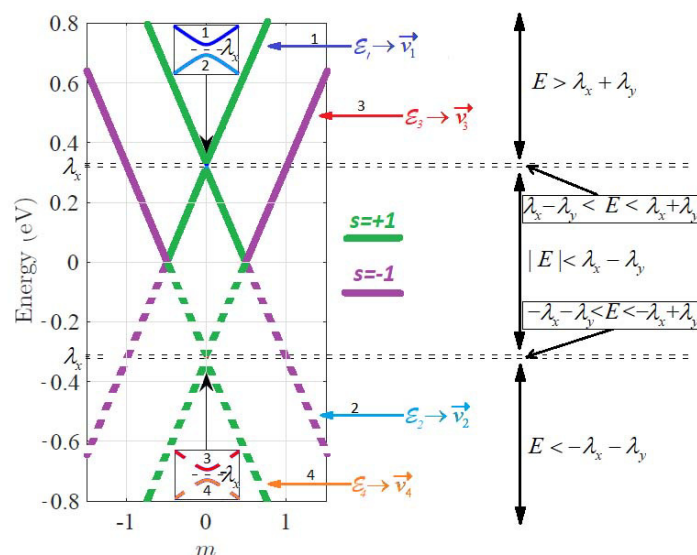


Figure 3. The same as in Figure 2. Solid lines are associated with the positive energy states ($E > 0$), while the negative energies are denoted by dashed lines (see text). Once the energy changes the sign, it affects the sign of the corresponding quantum number s . There are anticrossing of the energy branches with the same quantum number $s = +1$ for the pair $(\mathcal{E}_1, \mathcal{E}_2)$ at $E > 0$ and for the pair $(\mathcal{E}_3, \mathcal{E}_4)$ at $E < 0$.

At $k_y = 0$, the eigenvectors in Equation (5) of the Hamiltonian in Equation (1) transform to the following form (see details in [13,17]):

$$\Phi_{j,m}(\theta) = \left(I \otimes e^{-i\frac{\sigma_y}{2}\theta} \right) \vec{v}_j(m) e^{im\theta}, j = 1, \dots, 4. \quad (42)$$

Here

$$\vec{v}_1 = \begin{pmatrix} -it_m \\ -A_- \\ -iA_- \\ -t_m \end{pmatrix}, \vec{v}_2 = \begin{pmatrix} -it_m \\ A_+ \\ iA_+ \\ -t_m \end{pmatrix}, \vec{v}_3 = \begin{pmatrix} -it_m \\ A_+ \\ -iA_+ \\ t_m \end{pmatrix}, \vec{v}_4 = \begin{pmatrix} -it_m \\ -A_- \\ iA_- \\ t_m \end{pmatrix}, \quad (43)$$

where

$$A_{\pm} = \pm\lambda_y + \sqrt{t_m^2 + \lambda_y^2}. \quad (44)$$

The choice of the components of the wave function in Equation (42) depends on the energy interval in Equation (37), available for electrons. For example (see Figure 2), for $E > \lambda_x \Rightarrow E = \mathcal{E}_1 \vee E = \mathcal{E}_3$, the base eigenfunctions are: $\sim \exp(\pm im_{+1}\theta) \vec{v}_1(\pm t_{m_{+1}}); \sim \exp(\pm im_{-1}\theta) \vec{v}_3(\pm t_{m_{-1}})$, respectively. As discussed above, the quantum number s , characterising the components of the wave function in Equation (42), is associated with the specific energy (see Equations (40) and (41)). The wave function in Equation (13) of the flat graphene at $k_y = 0$ is convenient to present in the form:

$$\Psi_k^\sigma(x) = \frac{1}{2} \begin{pmatrix} \tau \frac{k}{|k|} \\ 1 \end{pmatrix} \otimes \begin{pmatrix} 1 \\ \sigma i \end{pmatrix} e^{ikx}, \quad \sigma = \pm. \quad (45)$$

As above, we use the following definitions: $\Psi_k^\sigma(x) \equiv \langle x | \sigma, k \rangle$, $\sigma = (+/-) \Leftrightarrow \sigma = (\uparrow / \downarrow)$. The symbol $\tau = -(+)$ is ascribed to the valence (conduction) band. We study the case $E \geq 0$; the opposite case can be analysed with the same method. As above, the positive value of the wave number $k \equiv k_x$ corresponds to the direction of the electron motion from the left to the right side of the considered system.

In the case $k_y = 0$, there is one more operator $\hat{S}_{ch} = \tau_x \otimes \sigma_y$ that commutes with both Hamiltonians in Equations (1) and (11), describing the flat and the rippled pieces of our system, respectively:

$$[\hat{S}_{ch}, H_f] = 0, \quad [\hat{S}_{ch}, H_r] = 0. \quad (46)$$

For the wave function, associated with the flat graphene sheet, we have

$$\left. \begin{aligned} \hat{S}_{ch} | \uparrow \pm k \rangle &= \pm | \uparrow \pm k \rangle \\ \hat{S}_{ch} | \downarrow \pm k \rangle &= \mp | \downarrow \pm k \rangle \end{aligned} \right\} \Rightarrow \alpha = \pm 1. \quad (47)$$

Thus, the operator \hat{S}_{ch} has the eigenvalue $\alpha = +1(-1)$, acting on the wave function of the electron, traveling from the left side of our structure with spin up (down) polarisation. The eigenvalues are equal in value but opposite in sign if the operator \hat{S}_{ch} acts on the wave function of the electron, traveling from the right side of our structure with spin up (down) polarisation. On the other hand, the action of the operator \hat{S}_{ch} on the electron wave functions, associated with the rippled piece of our system, is as follows:

$$\hat{S}_{ch} \Phi_{1,m}(\theta) = -\Phi_{1,m}(\theta), \quad (48)$$

$$\hat{S}_{ch} \Phi_{2,m}(\theta) = -\Phi_{2,m}(\theta), \quad (49)$$

$$\hat{S}_{ch} \Phi_{3,m}(\theta) = +\Phi_{3,m}(\theta), \quad (50)$$

$$\hat{S}_{ch} \Phi_{4,m}(\theta) = +\Phi_{4,m}(\theta). \quad (51)$$

In this case, the operator \hat{S}_{ch} has the eigenvalue $\alpha = +1(-1)$ as well, providing us the connection between the eigenstates of the flat and rippled pieces of the considered system.

Now, we are ready to discuss the list of eigenfunctions, responsible for the transport properties in different energy range.

- $E > \lambda_x$.

1. *Quantum numbers:* $\alpha = +1, s = -1$. These quantum numbers determine the available set of the wave functions: $\Psi_k^+(x), \Psi_{-k}^-(x), \Phi_{3,m}(\theta)$. If the corresponding symmetries are responsible for the transport properties, there are only the following options.

- (a) The electron is moving from the left side of our structure (flat graphene sheet) with the spin up polarisation [$\Psi_k^+(x) \equiv |\uparrow +k\rangle$]. In this case, in the rippled graphene region (see Figure 2), there is one open channel, defined by the wave function $\Phi_{3,m}$. The wave function $\Psi_{-k}^-(x) \equiv |\downarrow -k\rangle$ describes the reflection with the electron spin-flip.
- (b) The electron is moving from the right side (flat graphene sheet) with the spin down polarisation [$\Psi_{-k}^-(x) \equiv |\downarrow -k\rangle$]. In this case, in the rippled graphene region, there is only the transmission channel, defined by the wave function $\Phi_{3,m}$. The wave function $\Psi_k^+(x) \equiv |\uparrow +k\rangle$ describes the reflection with the electron spin-flip.

As a result, we expect the equivalence between the left/right transmission probabilities with the opposite spin polarisations. Indeed, this expectation is consistent with Equation (33), obtained from the different arguments at $k_y = 0$.

2. *Quantum numbers:* $\alpha = -1, s = +1$. The available set of the wave functions: $\Psi_k^-(x), \Psi_{-k}^+(x), \Phi_{1,m}(\theta)$. In this case, the symmetries dictate the following options.

- (a) The electron is moving from the left side (flat graphene sheet) with the spin down polarisation [$\Psi_k^-(x) \equiv |\downarrow +k\rangle$]. In this case, in the rippled graphene region (see Figure 2), there is one open channel, defined by the wave function $\Phi_{1,m}(\theta)$. The wave function $\Psi_{-k}^+(x) \equiv |\uparrow -k\rangle$ describes the reflections with the electron spin-flip.
- (b) The electron is moving from the right side (flat graphene sheet) with the spin up polarisation [$\Psi_{-k}^+(x) \equiv |\uparrow -k\rangle$]. In this case, in the rippled graphene region for this electron there is only the transmission channel, defined by the wave function $\Phi_{1,m}(\theta)$. The wave function $\Psi_k^-(x) \equiv |\downarrow +k\rangle$ describes the reflections with the electron spin-flip.

Again, we expect the equivalence between the left/right transmission probabilities with the opposite spin polarisations. Indeed, this expectation is consistent with Equation (35), obtained from different arguments at $k_y = 0$.

- $E < \lambda_x$.

1. *Quantum numbers:* $\alpha = -1, s = +1$. In this case, the available set includes the following wave functions: $\Psi_{-k}^+(x), \Psi_k^-(x), \Phi_{2,m}(\theta)$. The symmetries dictate the following options.

- (a) The electron is moving from the left side (flat graphene sheet) with the spin down polarisation [$\Psi_k^-(x) \equiv |\downarrow +k\rangle$]. In the rippled graphene region, there is only the transmission channel, defined by the wave function $\Phi_{2,m}(\theta)$. The wave function $\Psi_{-k}^+(x) \equiv |\uparrow -k\rangle$ describes the reflections with the electron spin-flip.
- (b) The electron is moving from the right side (flat graphene sheet) with the spin up polarisation [$\Psi_{-k}^+(x) \equiv |\uparrow -k\rangle$]. In the rippled graphene region, there is only the transmission channel, defined by the wave function $\Phi_{2,m}(\theta)$. The wave function $\Psi_k^-(x) \equiv |\downarrow +k\rangle$ describes the reflections with the electron spin-flip.

Again, the expected equivalence between the left/right transmission probabilities with the opposite spin polarisations is consistent with Equation (35), obtained from different arguments at $k_y = 0$.

2. *Quantum numbers:* $\alpha = +1, s = -1$. In this case, the available set includes the following wave functions: $\Psi_k^+(x), \Psi_{-k}^-(x), \Phi_{3,m}(\theta)$. This situation is completely equivalent to the case discussed at $E > \lambda_x$, Point 1.

Thus, at $k_y = 0$, the symmetry, associated with the operator \hat{S}_{ch} , determines the following transport properties through the rippled graphene piece: (i) at the transmission, it preserves the electron spin polarisation, while forbids the spin-flip; and (ii) the reflection occurs only with the spin-flip.

For $k_y \neq 0$, the operator \hat{S}_{ch} does not commute with the Hamiltonians. In this case, the discussed symmetry is broken. It results in constraint release on the reflections and transmissions mechanisms in our system (i.e., [25]).

3.3. The Relation Between the Operators \hat{S}_t and \hat{S}_{ch}

Note that these two symmetry operator commute if $k_y = 0$. Evidently, they have the common basis, while having different eigenvalues. Let us analyse this situation in details. One can readily see that the eigenfunctions in Equations (18) and (19), associated with the flat graphene piece, are common eigenstates for the both operators:

$$\hat{S}_t|\psi_{\pm}\rangle = \pm|\psi_{\pm}\rangle, \quad \hat{S}_t|\phi_{\pm}\rangle = \pm|\phi_{\pm}\rangle, \quad (52)$$

$$\hat{S}_{ch}|\psi_{\pm}\rangle = +|\psi_{\pm}\rangle, \quad \hat{S}_{ch}|\phi_{\pm}\rangle = -|\phi_{\pm}\rangle. \quad (53)$$

For the rippled graphene piece, we have to consider only the case $k_y = 0$. In this case, it is convenient to construct the common basis from the set in Equation (42). Taking into account the properties in Equations (48)–(51), we introduce the following superpositions

$$\Phi_j = \frac{1}{2}[\Phi_{j,m}(\theta) + \Phi_{j,-m}(\theta)], \quad j = 1, \dots, 4. \quad (54)$$

As a result, we obtain

$$\hat{S}_t\Phi_{1,2} = \Phi_{1,2}, \quad \hat{S}_t\Phi_{3,4} = -\Phi_{3,4}, \quad (55)$$

$$\hat{S}_{ch}\Phi_{1,2} = -\Phi_{1,2}, \quad \hat{S}_{ch}\Phi_{3,4} = \Phi_{3,4}. \quad (56)$$

Thus, the eigenfunctions in Equation (54) form the complete set for the both symmetry operators in the case of the rippled graphene piece.

4. Summary

Evidently, symmetries play an essential role in our understanding different phenomena in mesoscopic physics. In graphene physics, they become especially apparent in the transport properties of the corrugated systems. We find two symmetry operators that explain the chiral behaviour of the ballistic electron transport through the rippled graphene. This unusual behaviour has emerged due to the curvature-induced spin–orbit coupling. In particular, the symmetry operator \hat{S}_t (see Section 3.1) elucidates the equivalence between the transport characteristics of the ballistic electrons travelling from opposite sides of our system that have different type of polarisations. This operator acts as a time-reversal operator in the single valley system, considered in our paper. The other symmetry operator \hat{S}_{ch} (see Section 3.2) enables us to explain the selection of open energy channels for the ballistic electrons travelling through the rippled graphene subsystem at the direct incident of the electron flow ($k_y = 0$). This symmetry explains the dominance of different electron spin polarisations that depend on the direction of the electron flow. This selection becomes increasingly important at multiple periodic

repetition of the corrugated graphene structure, considered in our paper (see also [14]). From our preliminary analysis, it follows that similar symmetry preserves if we consider the down side of the CNT. This problem is, however, beyond the scope of the present studies and will be discussed in detail in forthcoming paper.

Author Contributions: All authors contributed equally to this work. All authors have read and agreed to the published version of the manuscript.

Funding: This work is partially supported by the Slovak Academy of Sciences in the framework of VEGA Grant No. 2/0009/19, and by Votruba-Blokhintsev program BLTP, JINR.

Conflicts of Interest: The authors declare no conflict of interest.

References

1. Kumar, S.; Parks, D.M. Strain Shielding from Mechanically Activated Covalent Bond Formation during Nanoindentation of Graphene Delays the Onset of Failure. *Nano Lett.* **2015**, *15*, 1503–1510, doi:10.1021/nl503641c.
2. Cao, K.; Feng, S.; Han, Y.; Gao, L.; Hue, Ly, T.; Xu, Z.; Lu, Y. Elastic straining of free-standing monolayer graphene. *Nat. Commun.* **2020**, *11*, 284, doi:10.1038/s41467-019-14130-0.
3. Alyobi, M.M.; Barnett, C.J.; Rees, P.; Cobley, R.J. Modifying the electrical properties of graphene by reversible point-ripple formation. *Carbon* **2019**, *143*, 762–768, doi:10.1016/j.carbon.2018.11.076.
4. Vázquez de Parga, A.L.; Calleja, F.; Borca, B.; Passeggi, M.C.G.; Hinarejos, J.J.; Guinea, F.; Miranda, R. Periodically Rippled Graphene: Growth and Spatially Resolved Electronic Structure. *Phys. Rev. Lett.* **2008**, *100*, 056807, doi:10.1103/PhysRevLett.100.056807.
5. Maccariello, D.; Al Taleb, A.; Calleja, F.; Vázquez de Parga, A.L.; Perna, P.; Camarero, J.; Gnecco, E.; Farías, D.; Miranda, R. Observation of Localized Vibrational Modes of Graphene Nanodomains by Inelastic Atom Scattering. *Nano Lett.* **2016**, *16*, 2–7, doi:10.1021/acs.nanolett.5b02887.
6. Politano, A.; Chiarello, G. Plasmon modes in graphene: Status and prospect. *Nanoscale* **2014**, *6*, 10927–10940, doi:10.1039/C4NR03143A.
7. Ni, G.X.; Zheng, Y.; Bae, S.; Kim, H.R.; Pachoud, A.; Kim, Y.S.; Tan, C.L.; Im, D.; Ahn, J.H.; Hong, B.H.; et al. Quasi-Periodic Nanoripples in Graphene Grown by Chemical Vapor Deposition and Its Impact on Charge Transport. *ACS Nano* **2012**, *6*, 1158–1164, doi:10.1021/nn203775x.
8. Vasić, B.; Zurutuza, A.; Gajić, R. Spatial variation of wear and electrical properties across wrinkles in chemical vapour deposition graphene. *Carbon* **2016**, *102*, 304–310, doi:10.1016/j.carbon.2016.02.066.
9. Pudlak, M.; Nazmitdinov, R.G. Klein collimation by rippled graphene superlattice. *J. Phys. Cond. Matter* **2019**, *31*, 495301, doi:10.1088/1361-648X/ab3e8f.
10. Guinea, F.; Katsnelson, M.I.; Vozmediano, M.A.H. Midgap states and charge inhomogeneities in corrugated graphene. *Phys. Rev. B* **2008**, *77*, 075422, doi:10.1103/PhysRevB.77.075422.
11. Katsnelson, M.; Geim, A. Electron scattering on microscopic corrugations in graphene. *Philos. Trans. R. Soc. A Math. Phys. Eng. Sci.* **2008**, *366*, 195–204, doi:10.1098/rsta.2007.2157.
12. Ando, T. Spin-Orbit Interaction in Carbon Nanotubes. *J. Phys. Soc. Jpn.* **2000**, *69*, 1757–1763, doi:10.1143/JPSJ.69.1757.
13. Pudlak, M.; Pichugin, K.N.; Nazmitdinov, R.G. Cooperative phenomenon in a rippled graphene: Chiral spin guide. *Phys. Rev. B* **2015**, *92*, 205432, doi:10.1103/PhysRevB.92.205432.
14. Smotlacha, J.; Pudlak, M.; Nazmitdinov, R.G. Spin transport in a rippled graphene periodic chain. *J. Phys. Conf. Ser.* **2019**, *1416*, 012035, doi:10.1088/1742-6596/1416/1/012035.
15. Izumida, W.; Sato, K.; Saito, R. Spin-Orbit Interaction in Single Wall Carbon Nanotubes: Symmetry Adapted Tight-Binding Calculation and Effective Model Analysis. *J. Phys. Soc. Jpn.* **2009**, *78*, 074707, doi:10.1143/JPSJ.78.074707.
16. Del Valle, M.; Margańska, M.; Grifoni, M. Signatures of spin-orbit interaction in transport properties of finite carbon nanotubes in a parallel magnetic field. *Phys. Rev. B* **2011**, *84*, 165427, doi:10.1103/PhysRevB.84.165427.
17. Pichugin, K.N.; Pudlak, M.; Nazmitdinov, R.G. Spin-orbit effects in carbon nanotubes—Analytical results. *Eur. Phys. J. B* **2014**, *87*, 124, doi:10.1140/epjb/e2014-50076-6.
18. Michaeli, K.; Kantor-Uriel, N.; Naaman, R.; Waldeck, D.H. The electron's spin and molecular chirality—How are they related and how do they affect life processes? *Chem. Soc. Rev.* **2016**, *45*, 6478–6487, doi:10.1039/C6CS00369A.

19. Nazmitdinov, R.G. From Chaos to Order in Mesoscopic Systems. *Phys. Part. Nucl. Letts.* **2019**, *16*, 159–169, doi:10.1134/S1547477119030154.
20. Birman, J.; Nazmitdinov, R.; Yukalov, V. Effects of symmetry breaking in finite quantum systems. *Phys. Rep.* **2013**, *526*, 1–91, doi:10.1016/j.physrep.2012.11.005.
21. Foa Torres, L.E.F.; Roche, S.; Charlier, J.C. *Introduction to Graphene-Based Nanomaterials: From Electronic Structure to Quantum Transport*; Cambridge University Press: Cambridge, UK, 2014; doi:10.1017/CBO9781139344364.
22. Katsnelson, M.I. *Graphene: Carbon in Two Dimensions*; Cambridge University Press: Cambridge, UK, 2012; doi:10.1017/CBO9781139031080.
23. Sakurai, J.J. *Modern Quantum Mechanics, Revised Edition*; Addison-Wesley: Reading, MA, USA, 1994.
24. Bohr, A.; Mottelson, B. *Nuclear Structure*; Number v. 1 in Nuclear Structure; World Scientific: Singapore, 1998.
25. Busa, J.; Pudlak, M.; Nazmitdinov, R.G. On Electron Scattering through a Single Corrugated Graphene Structure. *Phys. Part. Nucl. Lett.* **2019**, *16*, 729–733, doi:10.1134/S1547477119060414.



© 2020 by the authors. Licensee MDPI, Basel, Switzerland. This article is an open access article distributed under the terms and conditions of the Creative Commons Attribution (CC BY) license (<http://creativecommons.org/licenses/by/4.0/>).